

Coupled caldera subsidence and stirring inferred from analogue models

BEN M. KENNEDY^{1*}, A. MARK JELLINEK¹ AND JOHN STIX²

¹Earth and Ocean Sciences, University of British Columbia, 6339 Stores Road Vancouver, BC V6T 1Z4, Canada

²Earth and Planetary Sciences, McGill University, 3450 University Street, Montreal, Quebec, H3A 2A7, Canada

*e-mail: Bkennedy@eos.ubc.ca

Published online: 25 May 2008; doi:10.1038/ngeo206

Caldera-forming eruptions can be explosive and lead to the eruption of phenomenal volumes of magma that can devastate the global environment¹. Such eruptions involve ground subsidence related to catastrophic sinking of a magma chamber roof, accompanied by buoyant flow of magma through a ring conduit around the sinking roof². Previous work points to a feedback between subsidence and eruption: eruption initiates subsidence of the chamber roof, which in turn drives the ongoing eruption³. Although subsidence-driven eruption dominates caldera evolution⁴, the coupled dynamics of subsidence and magma flow are poorly understood. Here, we use analogue models to show that, under most conditions, caldera subsidence is spatially and temporally variable, leading to complicated and vigorous magma stirring and mixing. On the basis of the experimental results and a scaling analysis, we construct a regime diagram that helps demonstrate how the coupled flow and subsidence are influenced by the fluid dynamics and geometry of the system. The vigorous stirring we infer can considerably modify the style of subsidence and can explain textural, petrological and geochemical variation in deposits that have been related to caldera-forming eruptions.

To elucidate the mechanics governing supervolcano eruptions, scientists use observations from ancient calderas^{2,4,5} and smaller active caldera-forming eruptions^{6,7}, and numerical, analytical and analogue models^{3,8–12}. So far, no physical models have addressed adequately the coupled subsidence and magma flow of caldera formation^{10–12}. Analogue mixing experiments with simple conduit geometries show that in the absence of viscosity variations, turbulence or time-dependence in the flow mixing is not possible^{12–15}. More recently, elegant axisymmetric numerical simulations have been used⁸ to investigate the time-dependent dynamics of eruptions driven by the subsidence of a piston with a fixed spatial position into an underlying chamber of elliptical cross-section. The enforced axisymmetric geometry and the absence of two-way coupling between the moving fluid and the subsiding block significantly oversimplify subsidence and fluid flow. Indeed analyses of natural examples of caldera-forming eruptions show that magma chamber roofs sink with significant components of tilting and rotation^{16,17}, and that dyke widths vary spatially^{18–21}. These observations are also apparent in experiments on caldera subsidence¹², implying that the coupled problem of flow and subsidence is intrinsically three dimensional. Accordingly, we present the first analogue experiments of coupled subsidence and flow that enable the three-dimensional time-dependent dynamics to emerge naturally.

In two sets of experiments, cylindrical and semicylindrical blocks (analogues for magma chamber roofs) of height h and diameter d are released into underlying cylindrical chambers of diameter D , containing aqueous corn-syrup solutions with viscosities and densities that we vary. Block subsidence occurs as a result of flow between the block and the wall of the surrounding tank through the annular gap (that is, ‘ring conduit’) of average width, $w = D - d$ (Fig. 1) and involves the net contributions of four types of motion (Fig. 1): vertical displacement, lateral displacement, vertical rotation or ‘tilting’ and azimuthal rotation about the centre of mass (Fig. 1). The contributions of each component of block motion vary during a single experiment, and thus the flow from the chamber through the ring conduit can be complex. Three dimensionless parameters characterize the nature and evolution of the subsidence, and the mechanics and structure of the resulting flow: a Reynolds number Re for the induced flow, a tilt number Ti and a subsidence number Su (Fig. 1). Re indicates the relative importances of inertial and viscous forces for flow, stirring and mixing, whereas Ti and Su are geometric parameters that describe the degrees of freedom governing the motion of the block (Fig. 1). Su varies as the chamber thickness declines during each experiment, and thus we characterize subsidence and the corresponding flow over a wide range of Re – Su parameter space appropriate to silicic caldera systems. Our dimensions, scaling and experimental details are outlined in Fig. 1 and expanded on in the Methods section below.

Figure 2 shows an analysis of three single-block experiments that capture the main features of the subsidence and flow regimes identified in 118 experiments. The experiments are conducted under low-, intermediate- and high- Re conditions, respectively. During subsidence, H declines whereas the azimuthally averaged ring conduit width, w , remains unchanged, and so Su increases.

At low Re , initially the block tilts ($\Delta\theta = +0.85$) during a small fraction of the subsidence time $t_p = 0.02$. The tilting then becomes inhibited by the walls of the chamber, and the block subsequently subsides in this tilted position, stirring unsteady laminar flow azimuthally around and up the ring conduit (Fig. 2a). At intermediate Su there is little further tilting ($\Delta\theta = +0.06$), subsidence continues and flow is directed away from the direction of tilt (Fig. 2b). As the block approaches the chamber floor, it slowly ($t_p = 0.8$) tilts back to horizontal ($\Delta\theta = -0.91$). Fluid is squeezed from the narrowing gap between the foundering block and the floor, with a transition towards vertical motions (Fig. 2c).

By contrast, at high Re (Fig. 2g–i), the block initially tilts less ($\Delta\theta = +0.3$ over $t_p = 0.25$), and flow in the ring conduit

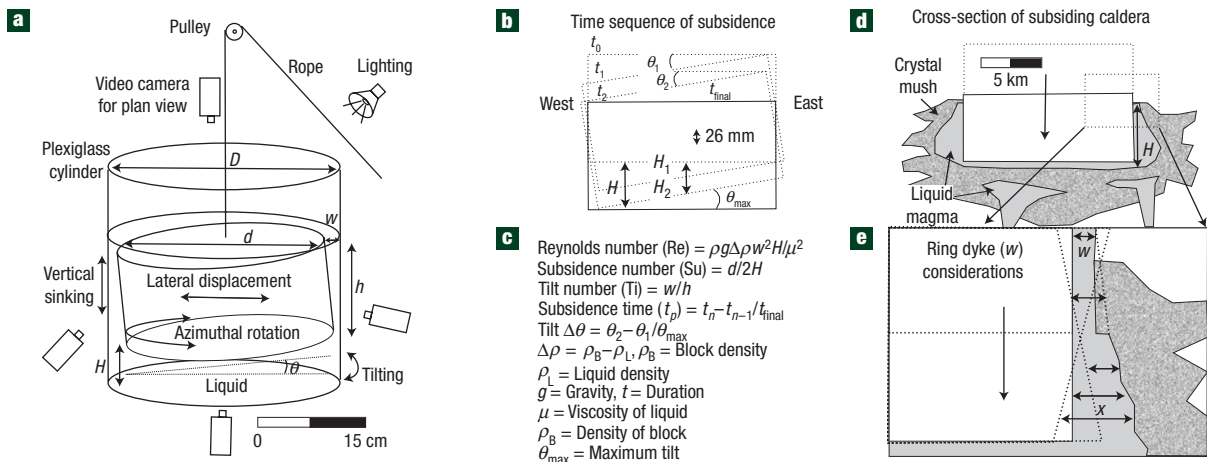


Figure 1 Details of experimental apparatus and scaling. **a**, Sketch of the experimental apparatus. **b**, A cross-sectional view of an experimental time sequence and the abbreviations that describe it. **c**, Dimensions and dimensionless numbers. **d**, A schematic cross-section through a natural system; note that H in the natural system is the height of dominantly liquid magma rather than the whole chamber. **e**, Ring dyke width in the natural system includes x , the diameter of the liquid portion of the chamber, and may be affected by the dip of ring faults.

is fully turbulent (Fig. 2g). The flow is predominantly vertical, characterized by eddies with maximum vertical length scales ranging between w and $h/2$. Extensive stirring and overturning are observed within the ring conduit (Fig. 2g). Subsidence continues and tilting is not inhibited by the walls (Fig. 2h). As the block approaches the floor it tilts back to horizontal ($\Delta\theta = -0.61$) relatively rapidly ($t_p = 0.58$), and intense vorticity in the ring conduit concentrates near the bottom of the block (Fig. 2i).

Flow and subsidence in the intermediate-Re case are spatially and temporally complex (Fig. 2d–f), typical for flows transitional between laminar and turbulent regimes²². Initially, transient eddies and waves along with unsteady overturning motions are observed within the ring conduit and the underlying chamber (Fig. 2d). As the block approaches the floor of the chamber, the azimuthal component of the motions is in the direction of tilt and notably stronger than in the high-Re case (Fig. 2f).

Figure 3 shows the results of a ‘two-block’ experiment, which is important because calderas commonly subside as multiple blocks²³. The two-block experiments are conducted under high-Re conditions, in which the eastern block is forced to subside relative to the western block. This causes a large-scale flow (Fig. 3a) that overturns and stirs the full depth and lateral extent of the chamber and the ring conduit (Fig. 3b).

Both Figs 2 and 3 illustrate synchronous changes in both the subsidence style and the stirring regime; these changes are summarized in a regime diagram (Fig. 4). The subsidence and flow regimes are coupled and controlled by Re and by proximity to the walls and chamber floor. The terms ‘free tilt’, ‘wall-inhibited tilt’ and ‘floor-governed tilt’ correspond respectively to stirring styles of ‘vertical stirring’, ‘azimuthal stirring’ and ‘combined stirring’ (Fig. 4). The underlying mechanics for these regimes are explored quantitatively below.

A striking feature of all Re regimes is that block subsidence involves a time-dependent combination of vertical and lateral displacement, rotation and tilting. Consequently, although mean w is constant, there are local variations in conduit width that induce spatially varying changes in the viscous (low-Re), turbulent (high-Re) or combined (intermediate-Re) drag stresses retarding flow from the chamber through the ring conduit. Indeed, we observe that flow rate is enhanced where the ring conduit is

widest and drag forces minimized. Therefore, flow generally focuses in sections of the ring conduit least affected by tilting, that is, with parallel walls. However, this is generally an unsteady and unstable process and produces local high velocities, which can induce stresses and torques on the block. In all regimes the lateral and azimuthal position of the block evolves until subsidence is complete, reflecting a two-way mechanical coupling between the foundering block and the flow.

An additional aspect of all Re regimes is a flow transition that occurs as the block approaches the floor (Fig. 2), consistent with expectations from lubrication theory²². As H becomes small relative to w , the effect of viscous drag at the floor is enhanced and so t_p increases. However, conservation of mass demands that the ratio of the flow rate from the chamber to the flow rate up the ring conduit will increase at high Su (where $H < w$). Thus at high Re vorticity is enhanced near the chamber floor, despite the increased t_p .

A final observation from Fig. 2 is that the maximum observed tilt is always less than θ_{\max} . This behaviour may be a consequence of the average drag force imparted to the sidewall of the foundering block as a result of flow in the ring conduit. From classical boundary-layer theory²², the drag force scales as $F_d^l \sim \text{Re}^{1/2}$ for laminar flows and as approximately $F_d^l \sim \text{Re}^{1/7}$ for fully developed turbulent flows, for a range of conditions appropriate to our experiments. These scaling relationships are plotted in Fig. 4 along with a summary of behaviour from 69 single-block experiments with tracer particles. Re regimes and Su values are in good agreement with laminar theory for $\text{Re} < O(10^4)$, and are consistent with the turbulent theory at higher Re, although this limit is not well constrained by our experiments. Comparison of the scaling with the data indicates that the transition from laminar to turbulent flow occurs for an Re of order 10^4 , which is in agreement with the qualitative observations in Fig. 2.

During an actual caldera-forming eruption, Re can evolve in time as Su increases from an initial value, Su_0 , in response to, for example, progressive opening, erosion²⁴ or infilling of the ring dyke, or to variations in the effective magma viscosity. The effective magma viscosity can increase or decrease over many orders of magnitude²⁵. Comparison of results from field^{18–21} and modelling studies²⁶ indicate that ring dyke widths can evolve by a factor of ten or more and thus strongly influence Re (Fig. 4b). By contrast,

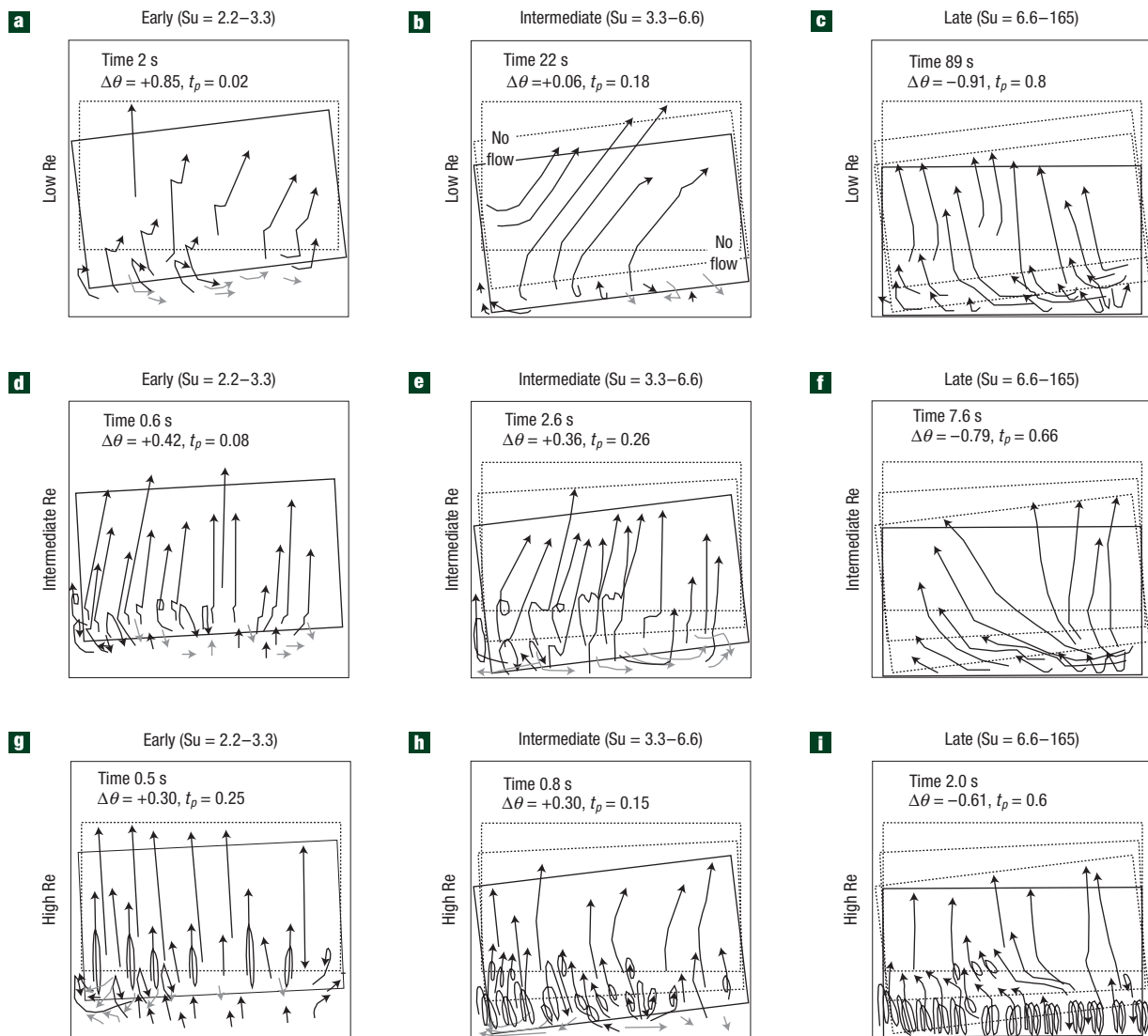


Figure 2 Experimental results for low (4.8×10^2), intermediate (1.9×10^3) and high (1.3×10^5) Re. **a**, Particle paths in the ring conduit have an easterly azimuthal component. **b**, Paths show no significant waves and continue to curve in an easterly direction. **c**, Paths change direction from easterly to westerly and form local low-amplitude waves. **d**, Paths are steep and frequently overturn locally. **e**, Paths overturn and kink. **f**, Paths in the ring conduit and chamber shift to westerly with a varying low angle. Inertial waves always occur, and overturning is observed in some experiments. **g**, Paths trace multiple overturns. **h**, Overturning becomes tighter. **i**, Overturning concentrates at the base of the ring conduit. Black arrows represent particle motion close to the front of the cylinder, and grey arrows represent particle motion in the centre of the cylinder.

variations in magma buoyancy are probably not much greater than a factor of two²⁵. To investigate the variation in Re–Su regimes during an eruption we assume a time evolution in these geometric and physical properties of the form $w, \mu, \Delta\rho \propto (Su/Su_0)^\beta$, where β varies depending on the process (see the Methods section; Fig. 4b).

To apply our results to specific natural cases we constrain Su_0 and characterize the subsidence style and eruptive products of the event. Long Valley Caldera is interpreted as a piston style caldera with an element of trapdoor subsidence²⁷, and so subsides in a manner similar to our single-block experiments. An appropriate Su_0 of 6 and Re_0 of 5,500 (see the Methods section) is shown in Fig. 4, indicating a transitional flow regime. The erupted Bishop Tuff records a vertical geochemical zonation in pumice-glass, crystal⁴ and melt-inclusion composition^{4,28}, whilst also revealing that different-temperature magmas from different depths in the

chamber mingled and erupted together^{2,24}. During the final stages of caldera collapse, the most heterogeneous and primitive magma erupted². Such a progressive increase in the extent of vertical mixing is consistent with the evolution in stirring expected as Su increases for constant Re (Figs 2 and 4). Moreover, if Re increases in response to dyke erosion and widening, the extent of heterogeneity is expected to be strongly enhanced as Su approaches a maximum value, which is observed. Other parameterizations for the evolution of the Bishop Tuff magma can be considered (see the Methods section), but overall the data can be well explained by our model.

The simultaneous eruption and mingling of magma from different depths in the chamber are recorded during many caldera-forming eruptions, although each eruption has a distinctive zonation pattern^{4,5,25,28–30}. Several ignimbrites associated with caldera-forming eruptions show highly heterogeneous vertical and

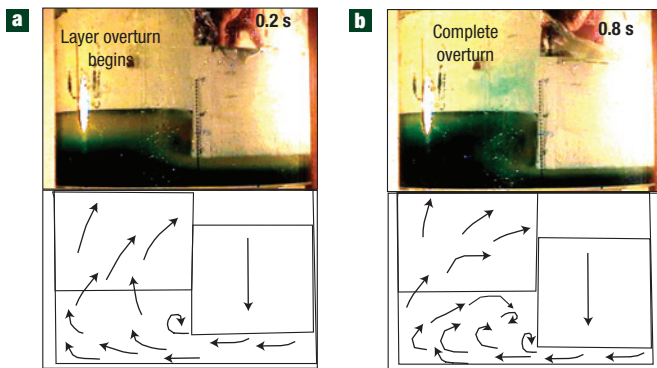


Figure 3 Photograph from the side of a two-block high-Re experiment. **a**, Fluid flows from under the eastern block into the western half of the chamber and begins to rise. As the eastern block descends, fluid overturns at its western margin. **b**, The westerly flowing fluid reaches the west chamber wall and rises, some fluid escaping directly up the ring conduit. The rest of the rising fluid encounters the base of the western block and overturns.

lateral chemical and textural zonation^{29,30}. Our experiments suggest that collapse on multiple blocks can drive large-scale overturn in the chamber (Fig. 3) and produce partially mingled heterogeneous magmas. Many other caldera collapse styles are possible; our experiments indicate that geometries of higher Re, additional tilt or multiple blocks will all tend toward more mingling and mixing.

Additionally, during a caldera-forming eruption, the final pulse of magma from the chamber floor remains in the ring fracture, solidifying to become a ring dyke. Ring dykes frequently contain mingled magma¹⁹. Our experiments imply that as the block settles on the magma mush pile (chamber floor) the most vigorous stirring will occur, whether the flow is laminar or turbulent (Fig. 2). Therefore, our experiments offer the first explanation for mingled and crystal-rich cumulate textures seen in natural ring dykes.

METHODS

Our regime diagram can be used to understand magma interaction expected over a range of caldera geometries and magma types, and during different collapse stages. Provided that $w \neq 0$ and tilt is possible (that is, $Ti \neq 0$), subsidence is expected to always be time dependent, affected by the evolving proximity of the subsiding block to the walls and the floor of the chamber. Concomitant magma flow is consequently always spatially and temporally complex, leading to extensive stirring in laminar, transitional and turbulent regimes. We suggest that collapse-driven magma mingling and mixing occurs during most caldera-forming eruptions, and that stirring can considerably modify the style of subsidence as well as the geochemistry and petrology of the erupted magma.

Before each experiment, working fluids are seeded with approximately neutrally buoyant particles, the motions of which are recorded with four video cameras positioned orthogonal to one another (Fig. 1). Particle path lines measured over the course of each experiment are used to characterize and quantify the structure of the fluid motions. Additional experiments with layered fluids of similar viscosities and densities but contrasting colour are also carried out to investigate qualitative mingling properties of the flows. In two-block experiments, the single cylindrical block is replaced by two semicylindrical blocks with the same total surface area.

We base our initial Ti (Ti_0) and Su (Su_0) on field observations of ring dykes and calderas^{3–5,17–21}. The initial Ti_0 is 0.08 and the initial Su_0 is 2.12 (that is, a natural caldera with a shallow, sill-like magma chamber, $d = 12$ km, liquid magma chamber thickness (H) = 2.83 km, depth of chamber (h) = 4 km and $w = 0.32$ km) (Fig. 1c). Ring dykes in nature vary from 10^1 to 10^3 m (refs 19–21) depending on the dip of ring faults (an outward-dipping ring fault

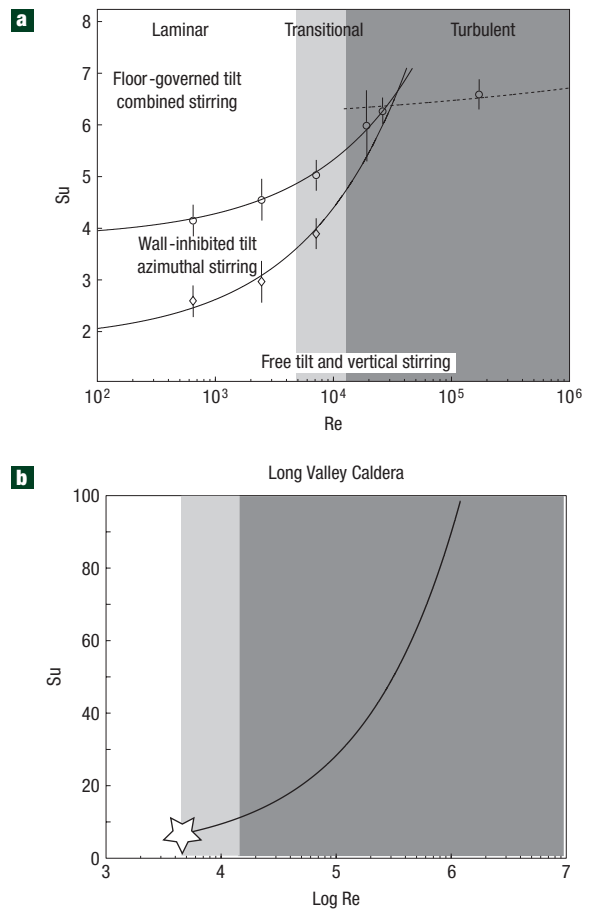


Figure 4 Regime diagrams. **a**, Experiments at six different Reynolds numbers; in the figure each experiment evolves vertically upwards with time as Su increases and the block sinks. Each data point is the mean of 9–14 experiments; diamonds and circles represent when the block first reaches the chamber sidewall and the floor, respectively. Curves are the expected relationships from classical boundary-layer theory for laminar and turbulent flows²². Subsidence and stirring regimes are also shown: ‘free tilt’ refers to roof tilting weakly influenced by the sidewall or floor; ‘wall-inhibited tilt’ refers to tilting strongly impeded by the sidewall; ‘floor-governed tilt’ refers to tilting controlled by the floor; ‘vertical stirring’ corresponds to a time-dependent (that is, unsteady) predominantly vertical flow; ‘azimuthal stirring’ corresponds to unsteady flow oriented $> 45^\circ$ from the vertical; ‘combined stirring’ corresponds to unsteady vertical and azimuthal motions. **b**, An example using data from Long Valley Caldera. The increase in Re during subsidence caused by widening of the ring dyke (30–400 m) in proportion to Su (that is, $Re \sim Su^{2\beta}$, where $\beta = 1$; see the Methods section). The star marks the initial Su_0 and Re_0 for Long Valley Caldera.

will progressively widen during subsidence) and additional differential between the ring fault diameter and the diameter of the liquid portion of the magma chamber (x) (Fig. 1d,e). In natural systems and in our experiments (Fig. 2), the critical w dimension is at the base of the ring dyke where overturning occurs; therefore, we use a diameter of 0.32 km typical for a deep ring dyke, which includes the dimension x (Fig. 1c) as opposed to the w dimension more appropriate for shallow ring dykes/faults^{19–21}.

For the specified Re, each experiment evolves from an initial value of $Su = 2.2$ towards a final value of order 100, corresponding to a minimum thickness of fluid trapped between the block and the rigid lower boundary, an artifact of the no-slip basal boundary condition. It is also useful to introduce the maximum tilt angle θ_{max} , which is measured to be $\pm 16.4^\circ$ for our system and can be obtained on geometric grounds from $D/d = 1 + [\sin^2(\theta_{max})/\cos(\theta_{max})]$. Uncertainties in the determination of Re are smaller than the symbols in

Fig. 4. Uncertainties in Su in Fig. 4a were calculated from differences in the mean measured H (when the block first touches the chamber floor) and a trigonometrically calculated H (constrained by θ and the floor).

Over the course of a supervolcanic eruption, the variation of Re caused by changes in dyke width and magma viscosity can be particularly extreme. The detailed temporal evolution of the geometric properties of the ring dyke and the physical properties of the magma imply complicated physical processes that may be coupled and thus not easily specified *a priori*. However, one way to parameterize the evolution of such effects is to assume that the time evolution is of the form $w, \mu, \Delta\rho \propto (Su/Su_0)^\beta$. Consequently, Re variation can be explored with the following relationships: dyke width $Re \propto w^2 \propto (Su/Su_0)^{2\beta}$, magma viscosity $Re \propto \mu^{-2} \propto (Su/Su_0)^{-2\beta}$ and changes in magma buoyancy $Re \propto \Delta\rho \propto (Su/Su_0)^\beta$. We propose that the range of geologically relevant conditions is set by assigning $-4 \leq \beta \leq 4$, say. The largest values of β imply superexponential temporal changes in Re and are taken as plausible end-member situations. However, variations may also be sudden, induced by stick-slip subsidence behaviour^{6,7} or by rapid changes in magma chemistry or temperature²⁵. For the special case of $\beta = 0$ for our experiments these properties are constant in time. In Fig. 4b, we plot $\beta = 1$, viscosity decrease or dyke-width increase proportional to time. For dyke erosion this value is conservative but enables us to explore a realistic parameter space. The relationships of dyke width $Re \propto w^2 \propto (Su/Su_0)^{2\beta}$ and magma viscosity $Re \propto \mu^{-2} \propto (Su/Su_0)^{-2\beta}$ also illustrate that high Re can occur at the end of subsidence, despite higher viscosities of crystal-rich magmas, if wide ring dykes form from conduit erosion, high values of x or outward-dipping faults (Fig. 1). Our investigation of the effect of dyke-width evolution at Long Valley Caldera uses the following values: $d = 20$ km, $H = 1.7$ km (the ratio of the minimum erupted volume to the caldera area), $30 < w < 400$ m, $h = 4$ km, $\rho = 2,300$, $\Delta\rho = 400$ kg m⁻³, $\mu = 5 \times 10^4$ Pa s (refs 4,27,28), giving a $Su_0 \approx 6$ and $Re_0 \approx 5,500$ (Fig. 4b). The Ti evolves from 0.01 to 0.1 as the ring dyke widens.

Received 27 September 2007; accepted 24 April 2008; published 25 May 2008.

References

- Rampino, M. & Self, S. Volcanic winter and accelerated glaciation following the Toba super-eruption. *Nature* **359**, 50–52 (1992).
- Fouqué, F. *Santorin et ses Eruptions* (Masson, Paris, 1879).
- Druitt, T. & Sparks, R. S. J. On the formation of calderas during ignimbrite eruptions. *Nature* **310**, 679–681 (1984).
- Hildreth, W. & Wilson, C. Compositional zonation in the Bishop Tuff. *J. Petrol.* **48**, 951–999 (2007).
- Druitt, T. H. & Bacon, C. R. Petrology of the zoned calcalkaline magma chamber of Mount Mazama, Crater Lake, Oregon. *Contrib. Mineral. Petrol.* **101**, 245–259 (1989).
- Simkin, T. & Howard, K. A. Caldera collapse in the Galapagos Islands, 1968. *Science* **169**, 429–437 (1970).
- Kumagi, H. *et al.* Very-long-period seismic signals and caldera formation at Miyake Island, Japan. *Science* **293**, 687–690 (2001).
- Folch, A., Codina, R. & Martí, J. Numerical modeling of magma withdrawal during explosive caldera-forming eruptions. *J. Geophys. Res.* **106**, 16163–16175 (2001).
- Trial, A. F., Spera, F. J., Greer, J. & Yuen, D. A. Simulations of magma withdrawal from compositionally zoned bodies. *J. Geophys. Res.* **97**, 6713–6733 (1992).
- Acocella, V. Understanding caldera structure and development: An overview of analogue models compared to natural calderas. *Earth Sci. Rev.* **85**, 125–160 (2007).
- Allen, J. J. & Chong, M. S. Vortex formation in front of a piston moving through a cylinder. *J. Fluid Mech.* **416**, 1–28 (2000).
- Blake, S. & Ivey, G. N. Magma mixing and the dynamics of withdrawal from stratified reservoirs. *J. Volcanol. Geotherm. Res.* **27**, 153–178 (1986).
- Blake, S. & Campbell, I. H. The dynamics of magma-mixing during flow in volcanic conduits. *Contrib. Mineral. Petrol.* **94**, 72–91 (1989).
- Koyaguchi, T. Magma mixing in a conduit. *J. Volcanol. Geotherm. Res.* **25**, 365–369 (1985).
- Ottino, J. *The Kinematics of Mixing: Stretching, Chaos and Transport* (Cambridge Univ. Press, Cambridge, 1989).
- Muira, D. Effects of changing stress states on the development of caldera-bounding faults: Geological evidence from Kumano caldera, Japan. *J. Volcanol. Geotherm. Res.* **144**, 89–103 (2005).
- Tucker, D. *et al.* Geology and complex collapse mechanisms of the 3.72 M Hannegan caldera, North Cascades, Washington, USA. *Geol. Soc. Am. Bull.* **119**, 329–343 (2007).
- Yoshida, T. Tertiary Ishizuki, cauldron, southwestern Japan arc: Formation by ring fracture subsidence. *J. Geophys. Res.* **89**, 8502–8510 (1984).
- Kennedy, B. & Stix, J. Magmatic processes associated with caldera collapse at Ossipee ring dike, New Hampshire. *Geol. Soc. Am. Bull.* **119**, 3–17 (2007).
- Sparks, R. S. J. Petrology and geochemistry of the Loch Ba ring-dyke, Mull (N.W. Scotland): An example of the extreme differentiation of tholeiitic magmas. *Contrib. Mineral. Petrol.* **100**, 446–461 (1988).
- McDonnell, S. *et al.* Intrusive history of the Slieve Gullion ring dyke, Ireland: Implications for the internal structure of silicic sub-caldera magma chambers. *Mineral. Mag.* **68**, 725–738 (2004).
- White, F. M. *Viscous Fluid Flow* (McGraw-Hill, New York, 1991).
- Heiken, G. *et al.* The Valles/Toledo caldera complex, Jemez Volcanic field, New Mexico. *Annu. Rev. Earth Planet. Sci.* **18**, 27–53 (1990).
- Druitt, T. H. Vent evolution and lag breccia formation during the Cape Riva eruption of Santorini, Greece. *J. Geol.* **93**, 439–454 (1985).
- Wolff, J. A., Woerner, G. & Blake, S. Gradients in physical parameters in zoned felsic magma bodies: Implications for evolution and eruptive withdrawal. *J. Volcanol. Geotherm. Res.* **43**, 37–55 (1990).
- Petford, N., Kerr, R. C. & Lister, J. R. Dike transport of granitoid magmas. *Geology* **21**, 845–847 (1993).
- Wilson, C. J. N. & Hildreth, W. H. The Bishop Tuff; new insights from eruptive stratigraphy. *J. Geol.* **105**, 407–439 (1997).
- Wallace, P. J., Anderson, A. T. & Davies, A. M. Gradients in H₂O, CO₂, and exsolved gas in a large-volume silicic magma system: Interpreting the record preserved in melt inclusions from the Bishop Tuff. *J. Geophys. Res.* **104**, 20097–20122 (1999).
- Bryan, S. Petrology and geochemistry of the quaternary caldera-forming, Phonolitic Granadilla Eruption, Tenerife (Canary Islands). *J. Petrol.* **47**, 1557–1589 (2006).
- Dreher, S. T., Eichelberger, J. C. & Larsen, J. F. The petrology and geochemistry of the aniakchak caldera-forming ignimbrite, Aleutian Arc, Alaska. *J. Petrol.* **46**, 1747–1768 (2005).

Acknowledgements

We thank R. Breger, T. Barton, A. Peterson, G. Robert and S. Wiingard for their assistance with experiments. Support was provided to B.M.K. from the Department of Earth and Planetary Sciences, McGill University, from GEOTOP, Université du Québec à Montréal and from the Canadian Institute for Advanced Research. A.M.J. acknowledges support from the Natural Sciences and Engineering Research Council of Canada, the Canadian Institute for Advanced Research and the Marsden Fund. J.S. acknowledges support from the Natural Sciences and Research Council of Canada and from le Fonds Québécois de la Recherche sur la Nature et les Technologies.

Author contributions

B.M.K., A.M.J. and J.S. all contributed to carrying out experiments and analysing data, as well as writing, planning and editing this manuscript.

Author information

Reprints and permission information is available online at <http://npg.nature.com/reprintsandpermissions>. Correspondence and requests for materials should be addressed to B.M.K.